
PALSAR InSAR Observation and Modeling of Crustal Deformation due to the 2007 Chuetsu-Oki Earthquake in Niigata, Japan

M. Furuya, Y. Takada

Department of Natural History Sciences, Hokkaido University, N10W8, Sapporo, 060-0810, Japan

Y. Aoki

Earthquake Research Institute, The University of Tokyo, Yayoi 1-1-1, Bunkyo, Tokyo, 113-0032, Japan

Abstract. On June 16 2007 (AM 10:13 in Japan Standard Time), an earthquake of magnitude 6.8 took place about 10 km offshore of Chuetsu area in Niigata, Japan..

Using L-band PALSAR InSAR (Interferometric Synthetic Aperture Radar) data, we could detect not only coseismic broad deformation but also significant aseismic deformation nearly 15 km away from the epicenter along an anticline axis. They mostly turned out to terminate within 3 days after the earthquake. The aseismic slip was modeled by a combination of west-dipping fault and east-dipping fault, which appear to be detachment faults on the western and eastern flank of the anticline. The moment magnitude released by the aseismic slip is estimated to be M_w 5.98. This observation demonstrates that a fault-related fold grows aseismically, and therefore seismic hazard is actually low for this particular fold. Although there is a dense GPS network in Japan, we should note that the aseismic signal was only detectable by InSAR data.

Keywords. Interferometric Synthetic Aperture Radar (InSAR), Advanced Land Observation Satellite (ALOS), L-band, Aseismic deformation, Anticline, Fold growth

1 Introduction

PALSAR is an L-band SAR sensor onboard ALOS (Advanced Land Observation Satellite), which was launched in January 2006 by Japan Aerospace Exploration Agency (JAXA). In contrast to other satellite SAR sensors, PALSAR uses a longer wavelength microwave, which is known to achieve good coherence even in densely vegetated areas

(Rosen et al. 1996). Meanwhile, there are more than 1200 GPS stations in Japan now. They were established with a goal of predicting earthquake and volcanic eruptions, and have been generating many interesting science results. Some people were in doubt about whether InSAR would be useful in understanding physics of earthquakes and volcanoes. In this paper, we show crustal deformation signals that could not be detected if PALSAR was unavailable. It was associated with an earthquake last year in Niigata, Japan. We call it Chuetsu-Oki earthquake; “Oki” stands for offshore in Japanese.

The Niigata basin is located at a diffuse plate boundary between Eurasian plate and North American plate (Fig. 1). Although there are no clear plate boundaries, GPS data indicate that a broad area from Niigata to Kobe is undergoing significant strain concentrations (Sagiya et al. 2000). Over the past 50 years, there have been a couple of large inland earthquakes (Fig. 1), and the 2007 Chuetsu-Oki earthquake is one of such events. Geologically, this area is known for active folding and thick sedimentary layer (Ikeda, 2002; Sato and Kato, 2005; Okamura et al. 2007). Our PALSAR InSAR data turned out to have important implications for active folding processes.

2 Data and Processing

We used four ascending and three descending PALSAR images, which cover the earthquake on July 16. The beam mode is FBS (fine beam single polarization), and the off-nadir angle is 34.3 degrees.

We have processed from level-1.0 PALSAR data, using Gamma software (Wegmüller and Werner, 1997). To eliminate topographic fringes, we used both 50-meter resolution digital elevation model (DEM) by Geographical Survey Institute, Japan, and

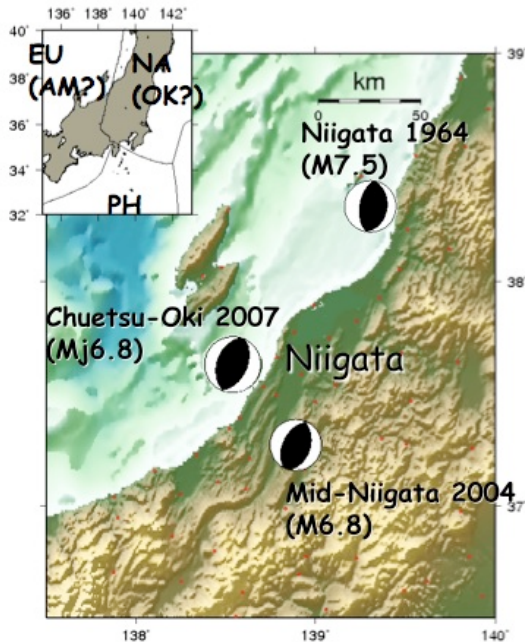


Fig. 1 Niigata area and three recent largest earthquakes. Inset shows tectonic plates around Japan.

15-meter resolution DEM generated from ASTER (Advanced Spaceborne Thermal Emission and Reflection Radiometer). For image registration prior to generating interferograms, we applied a so-called elevation dependent co-registration technique. While the phase-unwrapped results shown below are derived by minimum-cost-flow technique (Constantini, 1998), we confirmed that same results were obtained by branch-cut technique as well.

3 Observation Results

Fig. 2 shows results from descending track. The left two columns are covering the earthquake, and the right column is the result of post-seismic pair. We see that there was no significant post-seismic deformation. The difference of two rows is which digital elevation model was used to take out topographic fringes. Because ASTER DEM has finer spatial resolution, it could reveal more detailed signals. We should also note that the earliest post-earthquake image was acquired on July 19, which is 3 days after the event.

Fig. 3a shows a stack of descending interferograms; black dots indicate aftershocks. These broad signals near the coast are obviously due to the earthquake. Besides, we should note that there is a clear phase offset extending about 30 km.

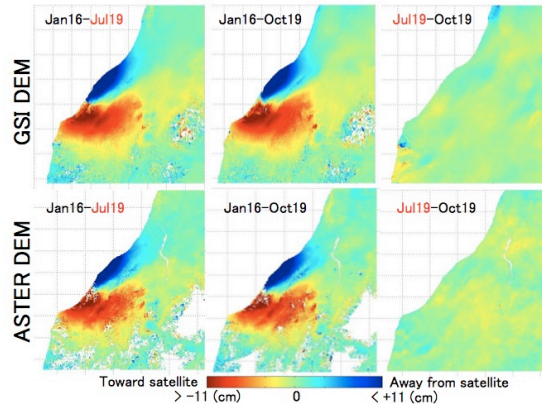


Fig. 2 PALSAR InSAR observation results for descending track, Path 60 and Frame 2860-2870.

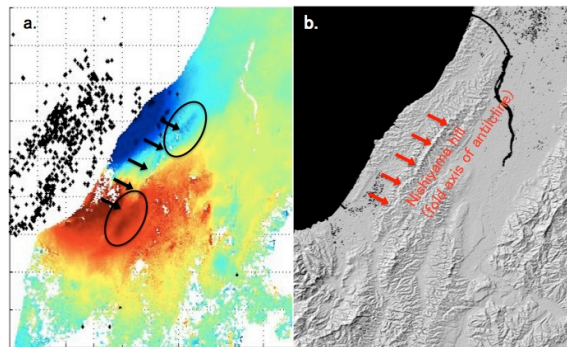


Fig. 3 (a) Stacked result of two descending images. Color scale is the same as in Fig. 2. (b) Shaded relief map. Arrows indicate Nishiyama hill.

Interestingly, the location closely matches a ridge called Nishiyama hill (Fig. 3b), which is thought to be an anticline axis. Also, despite the significant deformation, there are very few aftershocks. In other words, we have found that active folding occurs aseismically.

Figs. 4 show ascending interferograms. Now, the deformation signal near the anticline axis became much clearer. Unlike GPS, InSAR measures range changes in radar line of sight, and there is one caution in the interpretation of these InSAR data. For ascending track in this particular case, the GPS horizontal displacements are nearly perpendicular to the radar line of sight, and thus the ascending data is insensitive to horizontal motion. Thus, the range change amplitude is about a half of that in descending data. Fig. 5 is a stack of ascending interferograms. We can again observe broad signals along the coast and clear localized signals near the fold axis. Again, it should be noted that there are virtually no aftershocks near the anticline axis. These localized signals thus represent aseismic

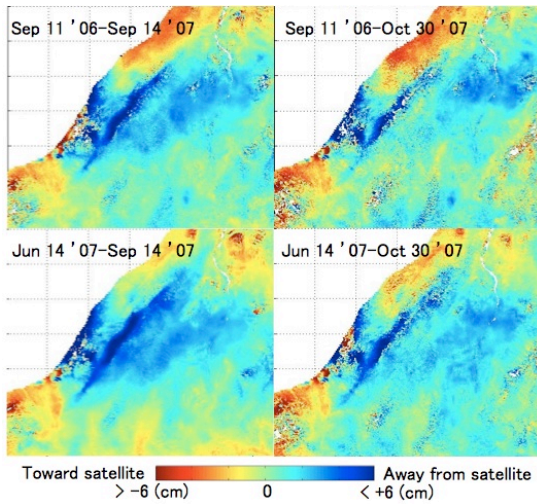


Fig. 4 PALSAR InSAR observation results for ascending track. Path 407 and Frame 730-740.

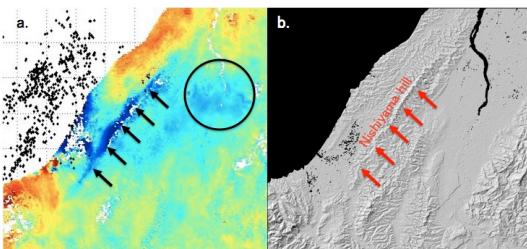


Fig. 5 (a) Stacked result of two ascending images. Color scale is the same as in Fig. 4. (b) Shaded relief map. Arrows indicate Nishiyama hill.

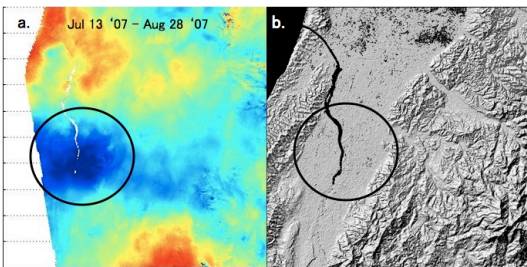


Fig. 6 (a) Another ascending image to the east. Color scale is the same as in Fig. 4. (b) Shaded relief map of the area.

deformation. Also, the small blob to the east is actually not an artifact by atmosphere in view of another adjacent ascending track to the east (Fig. 6). The signal pattern and the sense of deformation are consistent with the previous ascending images.

4 Modeling Results and Discussion

How do we interpret the observation? Our idea is that a main shock under the sea generates broad deformation signals near the epicenter, and that aseismic faults around the anticline axis caused localized signals. We infer these fault location, geometry and slip distribution, using the dislocation Green function by Okada (1992). Regarding the main shock fault, we assume a simple southeast dipping fault for the main shock, whose location and geometry are well constrained by aftershock data. For the aseismic fault, we must carefully set source faults. In Figs. 7 and 8, we show the actual contribution of aseismic deformation for both descending and ascending data. In order to understand what signals are expected depending on dip angles and to reproduce these aseismic signals, we carried out a simple forward modeling, and repeated numerous trials and errors. It turns out that the actual aseismic deformation is so complicated that we could not explain by a single fault. We propose a combination of both west dipping and east dipping faults in our modeling.

Fig. 7 is a modeling result for descending data. In the upper left, we show a map view of fault sources and aftershocks. The main-shock fault is offshore, and two inland faults are our preferred aseismic faults. One is northwest dipping and the other is southeast dipping. In the calculated interferogram, we see that not only the broad signal but also localized signals near the fold axis are well reproduced. Contributions by the main shock and aseismic faults are also shown in Fig. 7. Unless we introduce these two aseismic faults, we cannot reproduce this observation. The residuals are mostly less than 2 cm, and the agreement is quite good.

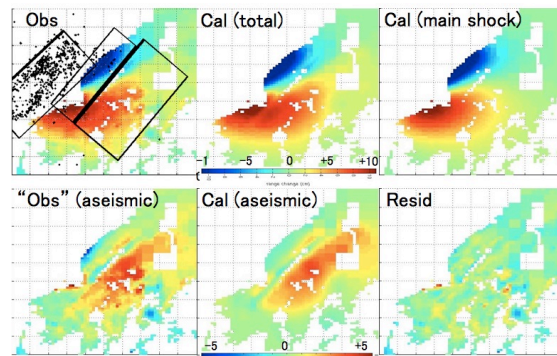


Fig. 7 Comparison of observed and modeled descending interferogram. See Fig. 9 for fault geometry.

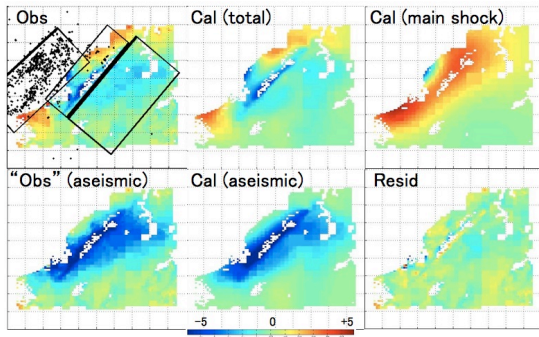


Fig. 8 Comparison of observed and modeled ascending interfergram.

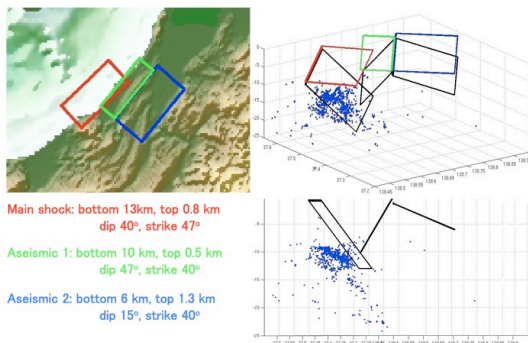


Fig. 9 Location and geometry of main shock fault (red) and two aseismic faults (blue and green).

Fig. 8 is a modeling result for ascending data. The observed and calculated data look similar to each other. In case of ascending data, both main shock and aseismic faults are generating similar order of signal amplitude but reverse in their sign. The residuals between observation and calculation are again mostly less than 2 cm.

Fig. 9 shows location and geometry of our fault model. The bottom depth of the main shock fault is 13 km, and the top depth is 0.8 km where there are few aftershocks. The two aseismic faults are shallower, and have lower dip angle.

Fig. 10 shows slip distributions for the main shock (Fig. 10a) and aseismic slip (Fig. 10b). The inferred moment magnitude for the main shock is M_w 6.62 with rigidity of 30 GPa. This value itself is quite consistent with a number of seismological estimates (Aoi et al. 2007; Hikima and Koketsu, 2007; Yamanaka, 2007; Yagi, 2007). Fig. 10b shows slip distribution for aseismic faults, and the estimated moment magnitude is M_w 5.96 and 5.98 for northwest and southeast dipping aseismic fault. According to the geometry, they appear to be

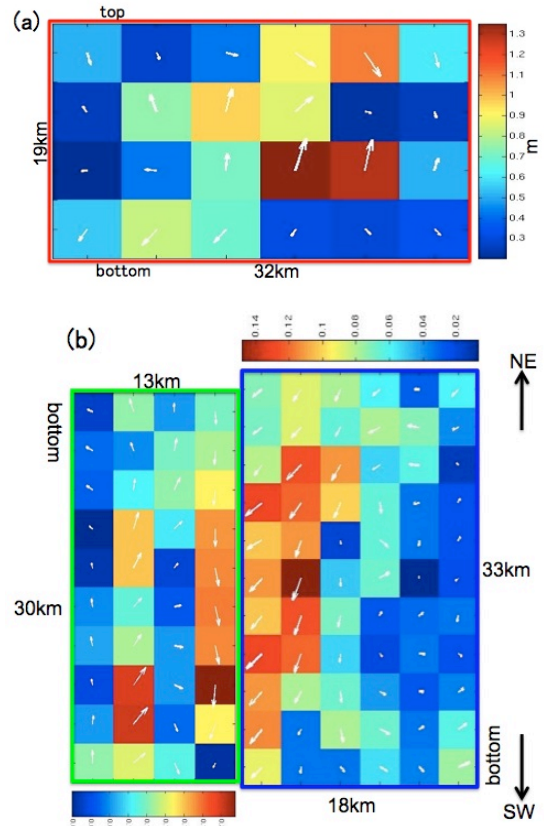


Fig. 10 Slip distribution on fault sources. (a) Main shock fault, (b) Two aseismic faults. See Fig.9 for their location and geometry. Unit of slip is in meter

detachment faults, connecting to the anticline axis. In view of the inferred slip distribution, there are some dip slip components in the deeper part. However, at the shallowest part, strike slip components are dominating, and the slip direction is similar in both northwest and southeast dipping fault. Our estimate of aseismic slip demonstrates that folds are caused not only by pure dip slip but also by strike slip motion.

Recently, using almost the same PALSAR InSAR data, Nishimura et al. (2008) estimated that the moment release due to the aseismic slip was M_w 4.2, which is overwhelmingly smaller than our estimate. Although the original SAR data is the same as ours, we notice that the Figure 2 in Nishimura et al is significantly different from our corresponding data in Figs. 7 and 8. In particular, while our aseismic "observed" range changes are broadly distributed (see lower-left in Fig.8), Nishimura et al's data are localized only around the anticline axis. We think that probably due to this difference in deformed area

in the ascending image, the big difference in the estimated moment release did come out. In other words, the fault model for the main shock must be different from ours, but Nishimura et al. (2008) did not show their main shock model. The main shock fault would significantly change the signals in ascending data.

Actually, our study is not the first detection of aseismic deformation of a fold-and-thrust belt. Fielding et al. (2004) reported such a signal associated an earthquake of magnitude 6.9. However, the post earthquake SAR image in their study was acquired 6 months after the event. Thus, it remained uncertain when the aseismic slip took place.

To answer this question, please recall that the earliest post-earthquake image was acquired 3 days after the event. We also examined daily GPS coordinates from the permanent GPS network. We found that the crustal deformation associated with this earthquake terminated mostly within 3 days. Therefore, it turns out that aseismic slip associated with fault-related folding is not as slow as a so-called slow earthquake that would take months or more (e.g., Ide et al. 2007; Furuya and Satyabala, 2008), but not as fast as generating short-period elastic waves. This might be a good news for local residents near fold belt, since seismic hazard potential should have been lowered.

Acknowledgement

The ownership of PALSAR data belongs to JAXA/METI. PALSAR level 1.0 data are shared among PIXEL, and provided from JAXA under a cooperative research contract with ERI, Univ. Tokyo. Hypocenter data was provided from Dr. Aitaro Kato. ASTER DEM is based on ASTER data beta processed by the AIST GEO Grid from ASTER data owned by METI. MF and YT are supported from the grant-in-aid for scientific research, JSPS (19340123).

References

Aoi, S., H. Sekiguchi, N. Morikawa, T. Kunugi, and M. Shirasaka (2007), Source Process of the 2007 Niigata-ken Chuetsu-oki Earthquake Derived from Near-fault Strong Motion Data, http://www.k-net.bosai.go.jp/k-net/topics/chuetsuoki20070716/inversion/ksw_ver070816_NIED_Inv_eng.pdf

- Constantini, M., (1998). A novel phase unwrapping method based on network programming, *IEEE Transactions on Geoscience and Remote Sensing*, 36, 813-821.
- Fielding, E.J., Wright, T.J., Muller, J., Parsons, B.E., and R. Walker (2004), Aseismic deformation of a fold-and-thrust belt imaged by synthetic aperture radar interferometry near Shahdad, southeast Iran: *Geology*, 32(7), 577-580.
- Furuya M., and S. P. Satyabala (2008), Slow earthquake in Afghanistan detected by InSAR, *Geophys. Res. Lett.*, 35, L06309, doi:10.1029/2007GL033049.
- Hikima, K. and K. Koketsu (2007), Source Process of the 2007 Niigata-ken Chuetsu-oki Earthquake (in Japanese) <http://taro.eri.u-tokyo.ac.jp/saigai/chuetsuoki/source/index.html>
- Ide, S., Beroza, G. C., Shelly, D. R. and T. Uchide (2007), A scaling law for slow earthquakes, *Nature*, 447, doi:10.1038/nature05780.
- Ikeda, Y. (2002). The Origin and mechanism of active folding in Japan, *Active Fault Research*, 22, 67-70 (in Japanese with English abstract).
- Nishimura T., M. Tobita, H. Yurai, T. Amagai, M. Fujiwara, H. Une, M. Koarai (2008), Episodic growth of fault-related fold in northern Japan observed by SAR interferometry, *Geophys. Res. Lett.*, 35, L13301, doi:10.1029/2008GL034337.
- Okada, Y. (1992), Internal deformation due to the shear and tensile faults in a half-space, *Bull. Seismo. Soc. America*, 82, 1018-1042.
- Okamura Y., T. Ishiyama, Y. Yanagisawa (2007), Fault-related folds above the source fault of the 2004 mid-Niigata Prefecture earthquake, in a fold-and-thrust belt caused by basin inversion along the eastern margin of the Japan Sea, *J. Geophys. Res.*, 112, B03S08, doi:10.1029/2006JB004320.
- Rosen, P, S. Hensley, H. Zebker, F. Webb, and E. Fielding (1996), Surface deformation and coherence measurements of Kilauea Volcano, Hawaii, from SIR-C radar interferometry, *J. Geophys. Res.*, 101(E10), 23109-23125.
- Sagiya, T., S. Miyazaki, and T. Tada (2000), Continuous GPS Array and Present-day Crustal Deformation of Japan, *PAGEOPH*, 157, 2303-2322.
- Sato, H. and N. Kato (2005). Relationship between geologic structure and the source fault of the 2004 Mid-Niigata Prefecture EarthquakeT, central Japan, *Earth Planets Space*, 57, 453-457.
- Wegmüller, U. and C. Werner (1997), Gamma SAR processor and interferometry software, In *Proc. the 3rd ERS Symposium*, ESA SP-414, 1686-1692.
- Yagi, Y. (2007), Source Process of the 2007 Niigata-ken Chuetsu-oki Earthquake, www.geol.tsukuba.ac.jp/~yagi-y/EQ/2007niigata/index.html
- Yamanaka, Y. (2007), Source Process of the 2007 Niigata-ken Chuetsu-oki Earthquake (in Japanese), www.seis.nagoya-u.ac.jp/sanchu/Seismo_Note/2007/NGY2a.html